



Comparison of lung imaging using three-dimensional ultrashort echo time and zero echo time sequences: preliminary study

Kyungsoo Bae^{1,2} · Kyung Nyeo Jeon^{1,2}  · Moon Jung Hwang³ · Joon Sung Lee³ · Ji Young Ha² · Kyeong Hwa Ryu² · Ho Cheol Kim⁴

Received: 2 July 2018 / Revised: 29 September 2018 / Accepted: 13 November 2018 / Published online: 13 December 2018
© European Society of Radiology 2018

Abstract

Objective To determine the feasibility of using high-resolution volumetric zero echo time (ZTE) sequence in routine lung magnetic resonance imaging (MRI) and compare free breathing 3D ultrashort echo time (UTE) and ZTE lung MRI in terms of image quality and small-nodule detection.

Materials and methods Our Institutional Review Board approved this study. Twenty patients underwent both UTE and ZTE sequences during routine lung MR. UTE and ZTE images were compared in terms of subjective image quality and detection of lung parenchymal signal, intrapulmonary structures, and sub-centimeter nodules. Differences between the two sequences were compared through statistical analysis.

Results Lung parenchyma showed significantly ($p < 0.05$) higher signal-to-noise ratio (SNR) in ZTE than in UTE. The SNR and contrast-to-noise ratio (CNR) of peripheral bronchus and small pulmonary arteries were significantly (all $p < 0.05$) higher in ZTE. Subjective image quality evaluated by two independent radiologists in terms of depicting normal structures and overall acceptability was superior in ZTE ($p < 0.05$). The diagnostic accuracy for sub-centimeter nodules was significantly higher for ZTE (reader 1: AUC, 0.972; $p = 0.044$; reader 2: AUC, 0.946; $p = 0.045$) than that for UTE (reader 1: AUC, 0.885; reader 2: AUC, 0.855). Mean scan time was 131 s (125–141 s) in ZTE and 467 s (453–508 s) in UTE. ZTE images were obtained with less acoustic noise.

Conclusion Implementing ZTE as an additional sequence in routine lung MR is feasible. ZTE can provide high-resolution pulmonary structural information with better SNR and CNR using shorter time than UTE.

Key Points

- Both UTE and ZTE techniques use very short TEs to capture signals from very short T2/T2* tissues.
- ZTE is superior in capturing lung parenchymal signal than UTE.
- ZTE provides high-resolution structural information with better SNR and CNR for normal intrapulmonary structures and small nodules using shorter scan time than UTE.

Keywords Lung · Magnetic resonance imaging · Ultrashort T2 · Ultrashort echo time · Zero-echo-time imaging

Abbreviations

AUC Area under the receiver operating characteristic curve
CNR Contrast-to-noise ratio

RF Radio frequency
ROI Region of interest
SI Signal intensity

Electronic supplementary material The online version of this article (<https://doi.org/10.1007/s00330-018-5889-x>) contains supplementary material, which is available to authorized users.

✉ Kyung Nyeo Jeon
knjeon@gnu.ac.kr

¹ Department of Radiology, Institute of Health Sciences, Gyeongsang National University School of Medicine, Jinju, South Korea

² Department of Radiology, Gyeongsang National University Changwon Hospital, 555 Samjeongja-dong, Seongsan-gu, Changwon 51472, South Korea

³ General Electronics (GE) Healthcare Korea, Seoul, South Korea

⁴ Department of Internal Medicine, Gyeongsang National University School of Medicine, Jinju, South Korea

SNR	Signal-to-noise ratio
TE	Echo time
UTE	Ultra-short echo time
ZTE	Zero echo time

Pulmonary MRI is a major challenge mainly due to the low proton density of the lung, inhomogeneity of magnetic susceptibility resulting from air and soft-tissue interfaces in the lung, and cardiopulmonary motions [1]. With conventional MRI sequences that use relatively long echo times (TEs), there is little opportunity to capture the rapidly decaying signal of lung tissue and small intrapulmonary structures that have very short T2/T2*.

With progress in MRI techniques, it becomes possible to visualize tissues containing very short T2 structures [2]. Ultra-short TE (UTE) is a new MRI technique that can acquire free induction decay at the end of the RF pulse as soon as possible by using a radial center-out k-space trajectory and short data sampling durations [3–5]. This allows better visualization of intrinsic MR signals of lung than conventional short-TE sequences [6]. Several studies using UTE have been conducted for quantitative and qualitative assessment of lung diseases such as emphysema and interstitial fibrosis [7–9]. Recently, the advanced 3D radial UTE technique that enables full coverage of the chest with isotropic high spatial resolution has been reported, providing images that resemble CT with excellent performance in the detection of small lung nodules [10].

Zero TE (ZTE) sequence is another MRI technique that can image tissues with ultrashort T2/T2* [11]. In this technique, readout gradients are turned on prior to RF excitation so that encoding can start simultaneously upon signal excitation, resulting in TE of nearly zero. With readout gradients on during RF excitation, flip angles and readout bandwidths are limited so that they would not affect imaging volume. Thus, the sequence is inherently 3D. With absence of rapidly switching gradients between TR intervals, ZTE can give additional benefits such as decreased acoustic noise [12]. With capability of reducing signal decay caused by T2* of lung parenchyma, this technique could be a promising tool in lung imaging. However, most previous studies using ZTE have been performed in head and musculoskeletal systems where involuntary motion is absent [11, 13, 14] while only very few studies have been conducted in lung imaging [15].

Detection of incidental lung nodules on chest CT commonly occurs in daily practice, with frequency of 15–30% [16]. Follow-up of some nodules with CT scans results in additional radiation exposure to patients. The Fleischner Society has announced revised recommendations for incidental lung nodules with increased size threshold to reduced unnecessary follow-up examinations [17]. However, alternative imaging modality without using ionizing radiation would be more beneficial to

patients, particularly for younger patients or those who require multiple examinations.

This study is motivated by questions about differences in lung images obtained using UTE and ZTE when both techniques similarly use very short TEs to capture signals from ultrashort T2/T2* tissues such as small intrapulmonary structures and sub-centimeter nodules. Although animal studies have suggested the promise of ZTE for lung imaging, structural imaging capability or quality of ZTE has not been evaluated in clinical studies yet [18]. To the best of our knowledge, no previous paper has compared UTE and ZTE images in lung MRI. Therefore, the goal of this study was to determine the feasibility of implementing respiratory-triggered high-resolution 3D ZTE in routine lung MRI. We also aimed to compare images obtained using UTE and ZTE in terms of depicting normal structures and sub-centimeter lung nodules.

Materials and methods

Patients

Our Institutional Review Board approved this study. Written informed consent was obtained from all patients before MR scans. From Nov. 2017 to Apr. 2018, 20 patients (males to females = 12:8) with mean age of 64.1 years (20–79 years) who underwent chest MRI for further evaluation of lung ($n = 15$) or mediastinal ($n = 5$) lesions detected on chest CT scans taken within 1–4 days before MRI were enrolled. UTE and ZTE sequences were performed additionally during the same scanning session of routine chest MRI.

Lung MR imaging

MR images were obtained using a commercial 3-T scanner (Signa Architect, GE Healthcare). UTE and ZTE scans were performed without contrast enhancement using a 36-channel body coil. UTE sequence used 3D cones trajectory which allowed flexible spiral-like read gradients [19]. ZTE sequence used silent scan algorithm (Silentz, GE Healthcare). Diagrams of UTE and ZTE sequences are shown in Fig. 1.

There were some differences between UTE and ZTE arising from their characteristics. However, we tried to keep similar conditions as much as possible between the two scans. In both sequences, 3D coronal images with isotropic resolution of 1.4 mm were obtained under free breathing. Respiratory motion was minimized by using respiratory triggering technique with the same threshold to accept end expiratory data for both sequences. While ZTE sequence characteristic limited flip angles (1–3°) and receiver bandwidth, UTE could use higher flip angles. Parameters of UTE and ZTE sequences are shown in Table 1. Acoustic noise levels were measured for each sequence using a MR-compatible sound level meter

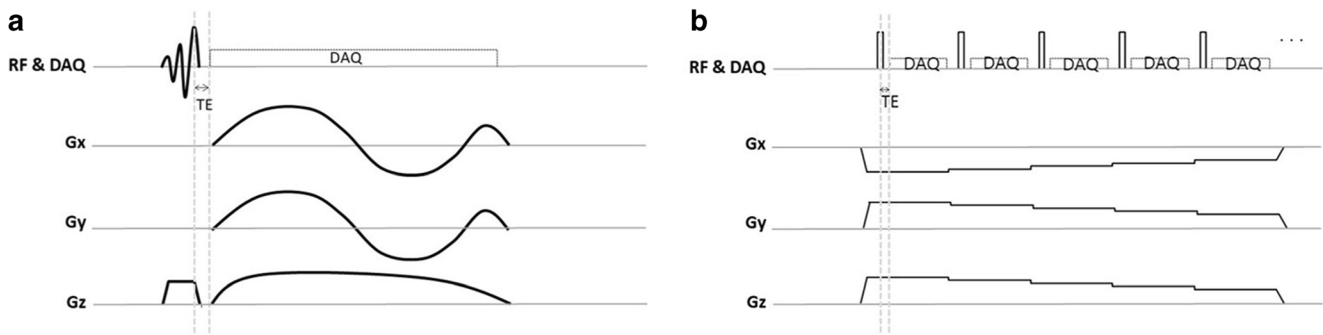


Fig. 1 Diagram of UTE and ZTE pulse sequences. **a** Pulse diagram of UTE (3D cones) sequence. The sequence can apply slice selection gradient which allows slab selection, higher flip angles, and higher bandwidths. The cone's trajectory allows for flexible spiral-like read gradients. DAQ, data acquisition. **b** Pulse diagram of a segment of ZTE sequence showing an example of five spokes in one segment. Two

(OptiSLM-100A-F, Optoacoustics Ltd) at a 2-m distance from the scanner in the closed room.

Image analysis

Original 3D coronal image data of UTE and ZTE were reconstructed into axial images. After image acquisition parameters and the name of sequences were removed, image datasets were transferred to the PACS system (Universal Viewer 6.0; GE Healthcare). Axial images were used for analysis.

To provide standard reference in lesion assessment, two radiologists (with 22 and 16 years of experience in chest CT, respectively) evaluated patients' chest CTs in consensus. CT scans were acquired with either a 64- or 320-MDCT scanner (IQon; Philips Healthcare or Aquilion ONE ViSION; Canon Medical Systems) utilizing a 2-mm slice thickness and 2-mm slice increment. In 7 of 20 patients, a total of 19 non-calcified

hundred fifty-six spokes per segment were applied in real scanning. Readout gradients are already ramped up before RF pulse followed by data acquisition (DAQ) resulting in a nominal zero echo time. This precludes application of slab selection. It also limits the maximum flip angle and readout bandwidth.

sub-centimeter-sized (2.8–9.7 mm, mean = 5.5 mm) solid nodules were detected on CT scan (1–4 nodule(s)/ patient). They were used in validation of UTE and ZTE for nodule evaluation. None of the non-calcified sub-centimeter nodules detected on CT was excluded from analysis because of their size or location.

Quantitative assessment of normal structures

To compare the ability of UTE and ZTE in detecting lung parenchymal signal and depicting normal structures, signal intensity (SI) of intrathoracic structures was measured and SNR and CNR were calculated. For this, two radiologists with 6 years and 8 years of experience in chest imaging, respectively, drew circular regions of interest (ROIs) in the background air, tracheal lumen air, lung parenchyma, trachea, peripheral bronchus, peripheral pulmonary artery, and aorta on each image dataset. The size of the ROI was adapted to the diameter of the structure, and the same size was applied for the same location in both sequences. All measurements were performed three times, and the mean was considered as the representative value of each structure.

When measuring the SI of the lung, vascular markings and fissures were avoided. For the SI of the trachea, the ROI was placed in the anterior or lateral tracheal wall without including luminal air. For the peripheral pulmonary artery, the circular ROI was drawn on a subsegmental or sub-subsegmental pulmonary artery appearing rounded on the image while the avoiding adjacent lung. For the peripheral bronchus, after selecting a segmental or subsegmental bronchus running perpendicular to the image plane, a circular ROI including the bronchial wall and luminal air was drawn on an image where the bronchus was delineated the best in each sequence.

To determine the ability of UTE and ZTE in detecting lung parenchymal signal, the SI of the background air, tracheal lumen air, and lung parenchyma were compared within each

Table 1 Parameters of UTE and ZTE sequences in lung MR of 20 patients

	UTE	ZTE
Acquisition type	3D, coronal	
FOV (isotropic)	400 × 400 mm	
Frequency	256	
Slice thickness	1.4 mm	
Number of slices	160–180 depending on the patient volume	
Acquisition resolution	1.4 mm iso-voxel	
Respiration trigger window	30	
Receiver bandwidth	± 125 kHz	± 41.7–± 62.5 kHz
Flip angle	8°	1–3°
No. of spokes per segment	1	256
Segment TR	5 ms	393–503 ms
ΔT (TE)	78 μs	16 μs
No. of average	1	1
Mean scan time (range)	467 s (453–508 s)	131 s (125–141 s)

sequence. The SNR of lung parenchyma was then compared between UTE and ZTE. To see differences in demonstrating mediastinal or intrapulmonary structures, the SNR of the trachea, peripheral bronchus, peripheral pulmonary artery, and aorta were compared between two sequences. CNRs of the peripheral bronchus and peripheral pulmonary artery were also compared. SNR was calculated as mean SI of measuring structure/noise. Standard deviation of the SI measured in the tracheal lumen was considered as noise. The CNR of the peripheral pulmonary artery was calculated as mean SI (pulmonary artery) – mean SI (lung)/noise. The CNR of the peripheral bronchus was calculated as mean SI (bronchus) – mean SI (lung)/noise.

Qualitative assessment of normal structures

Two cardiopulmonary radiologists (with 21 and 9 years of experience in chest imaging, respectively) independently evaluated UTE and ZTE images in terms of visualization of normal structures, degree of noise and artifacts, and overall acceptability. The score of each category was rated using a five-point scale (Table 2).

Assessment of sub-centimeter nodules

UTE and ZTE images were independently evaluated by two radiologists (with 12 and 6 years of experience in chest

Table 2 Qualitative grading system for assessment of lung MR images obtained using UTE and ZTE sequences

Depiction of the intrapulmonary vessels and fissures	
1, unacceptable (invisible peripheral pulmonary vessels and interlobar fissure)	
2, poor (barely visible peripheral pulmonary vessels/invisible interlobar fissure)	
3, fair (visible peripheral pulmonary vessels/invisible interlobar fissure)	
4, good (visible peripheral pulmonary vessels with clear margin/blurred interlobar fissure)	
5, excellent (visible peripheral pulmonary vessels with clear margin/sharp interlobar fissure)	
Depiction of the bronchus	
1, unacceptable (indistinguishable lobar bronchial walls)	
2, poor (visible lobar bronchial walls with few visible segmental bronchial walls)	
3, fair (visible segmental bronchial walls)	
4, good (visible subsegmental bronchial walls)	
5, excellent (visible sub-subsegmental bronchial walls)	
Image noise/artifacts (cardiac, respiratory, and streaking)	
1, unacceptable; 2, above-average noise/artifacts; 3, average and acceptable; 4, less than average; 5, minimum or nothing	
Overall acceptability	
1, unacceptable; 2, suboptimal; 3, satisfactory; 4, above average; 5, superior	

imaging, respectively) to detect sub-centimeter nodules. Two reading sessions were provided with 2-week interval to avoid consecutive reading of two sequences of the same patient. Twenty image data sets were presented on each session in random order. The number of true positive nodules was blinded to readers. First, readers were asked to record the presence or absence of sub-centimeter nodules on a lobe-by-lobe basis for each MR image data set. When there were multiple nodules in a lobe, only one dominant nodule in each lobe was included in the analysis. In the next step, readers were asked to assign one of five confidence levels to each decision as follows: 1, definitely absent; 2, probably absent; 3, possibly present; 4, probably present; or 5, definitely present.

For quantitative evaluation of nodules, the SI of nodules detected in both UTE and ZTE were measured by two radiologists with 6 years and 8 years of experience in chest imaging, respectively, using a circular ROI. SNR and CNR were calculated and compared between two sequences. The SNR of nodules was calculated as mean SI (nodule)/noise. The CNR of nodules was calculated as mean SI (nodule) – mean SI (lung)/noise.

Statistical analysis

Wilcoxon signed rank test was used to compare SI differences of the background air, tracheal lumen, and lung parenchyma within each sequence and differences of the CNR and SNR of normal structures and sub-centimeter nodules between UTE and ZTE. Image quality scores were also compared using Wilcoxon signed rank test. To evaluate the diagnostic accuracy of sub-centimeter nodules, receiver operating characteristic (ROC) curve analysis was performed and areas under the ROC curve (AUCs) were compared. McNemar's test was used to compare sensitivity of two sequences in nodule detection. To assess interobserver agreement for quantitative evaluation, intraclass correlation coefficient (ICC) was used. Interobserver agreement for qualitative assessment was determined by calculating the kappa coefficient. ICC or the kappa value was interpreted as follows: 0.20 or less, poor; 0.21–0.40, fair; 0.41–0.60, moderate; 0.61–0.80, substantial; and 0.81 or greater, almost perfect agreement. Statistical analyses were performed using MedCalc, version 17.6 (MedCalc Software) or SPSS package version 22.0 (SPSS Inc.). *P* values of less than 0.05 were considered to indicate statistical significance.

Results

All lung MR examinations were successfully performed without any adverse events. Figures 2 and 3 show typical UTE and ZTE images. The mean acquisition time was 467 s (453–508 s) for UTE and 131 s (125–141 s) for ZTE. Mean acoustic

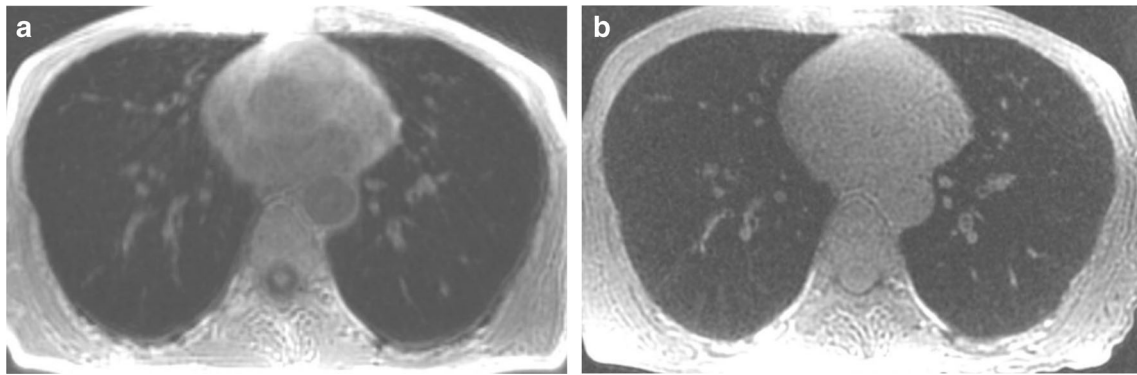


Fig. 2 Axial lung MR images at the level of both lower lobes obtained using UTE (a) and ZTE (b) sequences in a 57-year-old male. Intrapulmonary vessels and small bronchi are more clearly delineated in

ZTE image. Note the mediastinum and chest wall. While UTE demonstrates T1 contrast, ZTE shows proton density image, causing lack of contrast between structures

noise levels measured during ZTE and UTE scans were 50.2 dB and 82.4 dB, respectively. Background noise was 45.3 dB.

Quantitative assessment of normal structures

SIs of the background air, tracheal lumen air, and lung parenchyma were not significantly different in UTE by both readers. However, in ZTE, the SI of lung parenchyma was significantly higher than that of the background air or tracheal lumen air while SIs of the background air and tracheal lumen were not significantly different (Table 3).

SNRs of lung parenchyma, peripheral pulmonary artery, and peripheral bronchus were significantly (all $p < 0.05$) higher in ZTE by both readers. SNRs of the trachea and aorta were not significantly different between two sequences. CNRs of the peripheral pulmonary artery and peripheral bronchus were significantly (all $p < 0.05$) higher in ZTE by both readers (Fig. 4).

Interobserver agreements in measuring SIs of various structures were substantial for both sequences as follows: background air (ICC, 0.69 [95% CI 0.35, 0.80] in UTE; ICC, 0.71 [95% CI 0.51, 0.85] in ZTE), tracheal lumen air (0.76 [95% CI 0.48, 0.86] in UTE, 0.80 [95% CI 0.67, 0.89] in

ZTE), lung parenchyma (0.68 [95% CI 0.31, 0.83] in UTE, 0.75 [95% CI 0.56, 0.87] in ZTE), tracheal wall (0.71 [95% CI 0.46, 0.85] in UTE, 0.73 [95% CI 0.58, 0.87] in ZTE), peripheral bronchus (0.69 [95% CI 0.38, 0.84] in UTE, 0.71 [95% CI 0.54, 0.86] in ZTE), peripheral pulmonary artery (0.76 [95% CI 0.46, 0.86] in UTE, 0.72 [95% CI 0.48, 0.87] in ZTE), and aorta (0.79 [95% CI 0.57, 0.87] in UTE, 0.74 [95% CI 0.49–0.85] in ZTE). Noise measured in the tracheal lumen showed substantial agreements for both UTE (0.74 [95% CI 0.49–0.84]) and ZTE (0.76 [95% CI 0.66, 0.87]).

Qualitative assessment of normal structures

Subjective image quality scores for intrapulmonary structures were significantly higher in ZTE by both readers. Scores for noise were not significantly different between two sequences by both readers. Although scores for artifacts in ZTE were superior to those in UTE by both readers, the difference was significantly different only by reader 2. Overall acceptability scores were significantly higher in ZTE by both readers. The results are shown in Table 4.

When above score 3 was considered acceptable, UTE was acceptable in 16 patients by reader 1 and 15 patients by reader

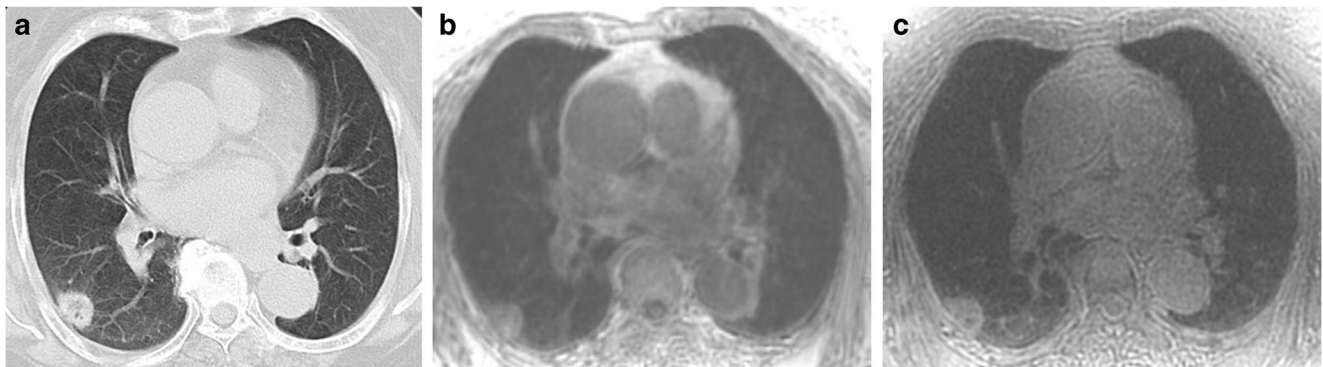


Fig. 3 Chest CT and lung MR images at the level of the left atrium in a 68-year-old female. Chest CT (a) shows a 2-cm-sized part-solid nodule in the right lower lobe superior segment. UTE (b) and ZTE (c) successfully

demonstrated the lesion. However, the internal character of the nodule was more consistent with that of CT on ZTE.

Table 3 Comparison of signal intensity of lung parenchyma, tracheal lumen air, and background air between UTE and ZTE sequences in lung MR

		ZTE					
UTE		Reader 2		Reader 1		Reader 2	
Lung (38.1 ± 5.4)	vs.	Lung (37.3 ± 3.9)	vs.	Lung (357.7 ± 126.1)	vs.	Lung (410.5 ± 127.0)	vs.
trachea (37.7 ± 7.9)	0.637	trachea (37.7 ± 7.9)	0.723	trachea (284.0 ± 89.3)	0.001*	trachea (290.9 ± 94.8)	0.001*
P 0.972		P 0.972		P 0.001*		P 0.001*	
		BG (36.5 ± 4.3)	vs.	BG (307.0 ± 94.7)	vs.	BG (410.5 ± 127.0)	vs.
		BG (36.5 ± 4.3)	0.637	trachea (284.0 ± 89.3)	0.079	trachea (290.9 ± 94.8)	0.615
		0.637		0.079		0.615	

Data are mean and standard deviation

Trachea tracheal lumen air, BG background air

*Difference is statistically significant

2 while ZTE was acceptable in 20 patients by reader 1 and 19 patients by reader 2.

Inter-reader agreements in the evaluation of vessels/fissures ($\kappa = 0.61$ in UTE, $\kappa = 0.70$ in ZTE), bronchus ($\kappa = 0.61$ in UTE, $\kappa = 0.71$ in ZTE), image noise ($\kappa = 0.79$ in UTE, $\kappa = 0.76$ in ZTE), artifacts ($\kappa = 0.59$ in UTE, $\kappa = 0.69$ in ZTE), and overall acceptability ($\kappa = 0.45$ in UTE, $\kappa = 0.63$ in ZTE) were substantial to moderate in both sequences.

Assessment of sub-centimeter nodules

In quantitative analysis for nodules detected in both sequences, CNR and SNR of sub-centimeter nodules were higher in ZTE by both readers (Table 5). However, only the difference of SNR was statistically significant. Interobserver agreements in measuring SIs of sub-centimeter nodules were substantial for UTE (ICC, 0.72 [95% CI 0.46, 0.87]) and ZTE (0.75 [95% CI 0.60, 0.88]).

The diagnostic accuracy for detecting sub-centimeter nodules on a per-lobe basis was significantly higher for ZTE (reader 1: AUC, 0.972 [95% CI 0.918, 0.995], $p = 0.044$; reader 2: 0.946 [95% CI 0.882, 0.981], $p = 0.045$) than that for UTE (reader 1: 0.885 [95% CI 0.806, 0.940], reader 2: 0.855 [95% CI 0.770, 0.917]) (Figs. 5 and 6).

When scores 3, 4, and 5 were considered positive, 14 and 16 nodules were detected on UTE by reader 1 and reader 2, respectively, while 17 nodules were detected on ZTE by each reader. The sensitivity was not significantly different between UTE and ZTE (73.7% vs. 89.5% for reader 1 and 84.2% vs. 89.5% for reader 2) by both readers.

Missed lesions in ZTE by both readers were smaller than 5 mm (2.6 mm and 4.3 mm). In UTE, two more nodules (5.7 mm and 3.2 mm) in the subpleural area were missed by reader 1 and a nodule (6.2 mm) in lingular segment was missed by both readers due to motion artifacts.

Discussion

MRI has not been frequently used for lung imaging since lung parenchyma has extremely short T2 and appears as signal void on conventional sequences. This limitation has been overcome with recently dedicated techniques that can directly image very short component such as UTE or ZTE, offering TE of < 1 msec. While the performance of UTE in the evaluation of lung parenchyma has been shown by several investigators, the feasibility study with ZTE has only been performed in healthy volunteers [8, 9, 15]. This is the first study comparing 3D UTE and ZTE sequences in lung MR for clinical patients. The signal of lung parenchyma was significantly higher than that of intratracheal air or background air in ZTE. The SNR of the lung parenchyma in ZTE was also superior to that in UTE. These results support exceptionally short T2/T2* capability of

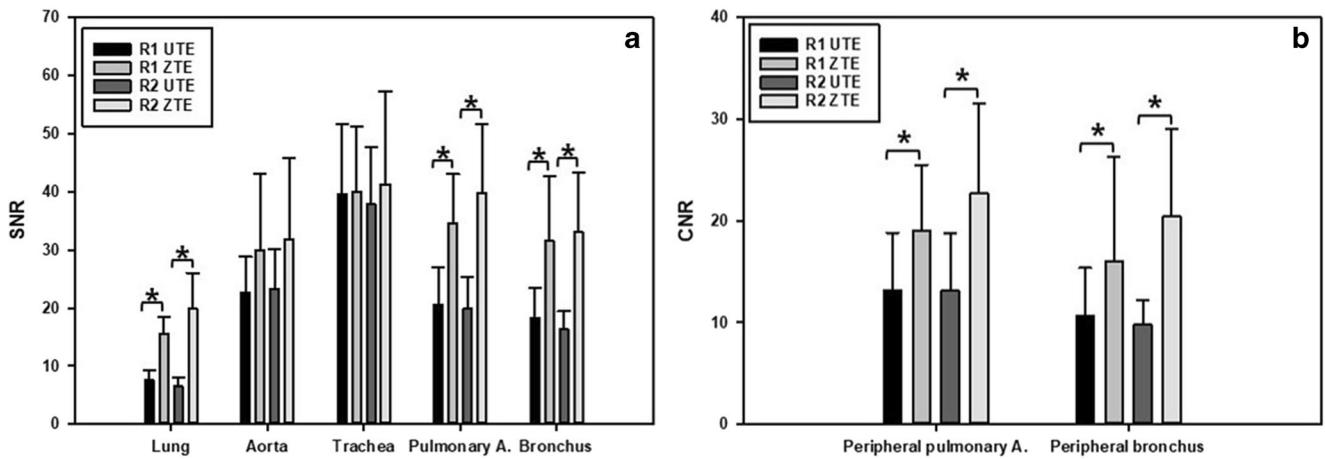


Fig. 4 **a** Graph comparing SNR of normal structures between UTE and ZTE sequences in lung MR. Data are mean and standard deviation. Asterisk, difference is statistically significant. R1, reader 1; R2, reader 2. **b** Graph comparing CNR of peripheral pulmonary artery and

peripheral bronchus between UTE and ZTE sequences in lung MR. Data are mean and standard deviation. Asterisk, difference is statistically significant. R1, reader 1; R2, reader 2

ZTE. Because data acquisition starts immediately after a short hard pulse with near-zero TE, very rapidly decaying transverse magnetization in the lung parenchyma can be captured more effectively with ZTE. This capability of ZTE in capturing lung parenchymal signal may be able to be applied in detecting and quantifying architectural disruption of the lung tissue such as emphysema [20].

ZTE is superior in depicting normal structures in the lung, including small vessels and peripheral bronchial walls. Considering that MR has a lower spatial resolution than CT and magnetic susceptibility of the lung, delineation of small peripheral bronchial walls in lung MRI is a challenging task. In this study, while the SNR and CNR of the trachea showed no significant differences between UTE and ZTE, those of the peripheral bronchus were significantly higher in ZTE. In subjective evaluation, the image quality scores of the peripheral bronchus were higher in ZTE. In spite of its similar tissue composition to the trachea, the peripheral bronchus in the lung may have a much shorter T2* than the trachea because of the surrounding lung tissue, particularly under higher field strength [21, 22]. The trachea resides in the mediastinum, being surrounded by vessels, the esophagus, and mediastinal

fat while the peripheral bronchus resides within the lung. Intrinsic magnetic susceptibility of the lung tissue can cause protons in the peripheral bronchus to undergo greater degrees of dephasing between excitation and readout stages [22, 23]. Therefore, ZTE with a shorter TE can be more advantageous in imaging the small bronchus and other fine intrapulmonary structures than UTE.

Non-contrast-enhanced lung MR as an alternative to CT in nodule detection has been investigated [24, 25]. The sensitivity of MRI for lung nodules larger than 8 mm in diameter is 100%. However, the sensitivity for smaller nodules varies depending on pulse sequences, nodule consistency, and breath holding condition [25]. Recently, high-resolution UTE imaging with a free-breathing technique has demonstrated promising results, comparable to low-dose chest CT [26, 27]. According to Burris NS et al [27], UTE has superior sensitivity for the detection of small (4–8 mm), non-FDG avid nodules than 3D dual-echo GRE sequence. Key differences were small voxel sizes and short TE. In our study, because the SI of surrounding lung parenchyma was also higher in ZTE, the CNR of sub-centimeter nodules was not significantly higher than that in UTE. However, ZTE showed higher SNR and

Table 4 Qualitative assessment of intrapulmonary normal structures and overall diagnostic acceptability of lung images obtained using UTE and ZTE sequences by two independent readers

	Reader 1			Reader 2		
	UTE	ZTE	p value	UTE	ZTE	p value
Vessels	2.9 ± 0.9	3.7 ± 0.7	0.001*	3.1 ± 0.8	3.9 ± 0.6	0.003*
Bronchus	3.1 ± 0.6	4.5 ± 0.5	0.001*	3.3 ± 0.6	4.6 ± 0.5	0.001*
Noise	3.6 ± 0.8	3.6 ± 0.6	0.655	3.4 ± 0.6	3.5 ± 0.7	0.655
Artifacts	3.4 ± 0.7	3.7 ± 0.5	0.096	3.4 ± 0.6	3.8 ± 0.6	0.034*
Overall acceptability	3.0 ± 0.7	4.1 ± 0.7	0.001*	3.0 ± 0.9	4.1 ± 0.8	0.005*

Data are mean and standard deviation

*Difference is statistically significant

Table 5 SNR and CNR of sub-centimeter nodules in UTE and ZTE lung MR images

	Reader 1			Reader 2		
	UTE	ZTE	<i>p</i> value	UTE	ZTE	<i>p</i> value
SNR	21.2 ± 4.6	34.3 ± 5.1	0.004*	22.5 ± 6.6	36.1 ± 6.9	0.017*
CNR	14.0 ± 4.4	16.6 ± 5.4	0.155	15.1 ± 5.6	17.5 ± 7.1	0.286

Data are mean and standard deviation

*Difference is statistically significant

readers' confidence for the presence of the nodule. Much shorter TE in ZTE might result in less signal loss of small nodules and higher readers' confidence. Readers missed two nodules in ZTE and three more nodules in UTE in the area prone to respiratory and cardiac motions. Although both sequences used the same free breathing technique, the motion artifact was more frequent in UTE due to a longer scan time. Since patients who undergo chest MRI often have poor pulmonary functions, they are unable to tolerate extensive examination times. Thus, scanning in a short time is requisite for good image quality in lung MRI. In the management of lung nodules, introduction of low-dose chest CT enables follow-up imaging with reduced radiation dose. However, patients who need repeated examinations might be harmed by cumulative radiation. Integration of ZTE in routine lung MR can provide high-resolution structural information, potentially avoiding the need for CT and associated radiation hazard.

Another advantage of ZTE was minimal acoustic noise during MR examinations. Fast current switches within the gradient coil can lead to vibration in their mountings and cause acoustic noise [28]. This noise is the most significant cause of discomfort during MRI examinations, particularly for children

or patients who are sensitive to acoustic noise [29]. Minimal gradient variations applied in the ZTE sequence can dramatically decrease acoustic noise and patient annoyance [30].

Despite those advantages, ZTE has several weaknesses in chest imaging. ZTE lacked appropriate image contrast for evaluation of long T2 tissues. Because the flip angle and allowed maximum receiver bandwidth were limited for a clinically reasonable scan time, ZTE images showed proton density contrast. It was limited for evaluating the mediastinum, chest wall structures, and internal character of large parenchymal lesions. Therefore, ZTE imaging should be performed as a complementary sequence to routine protocol instead of replacing conventional diagnostic sequences. In addition, oversensitive signal capturing and K-space sampling characteristics of ZTE might provoke lots of streak artifacts on images (Supplementary Figs. 1 and 2). Through experience with volunteer scans, we could improve image quality by using a small flip angle, a higher bandwidth, and a higher spatial resolution with enough coverage along the anterior to posterior direction in the coronal scan.

This study had several limitations. The main limitation is its small study population. Further studies with

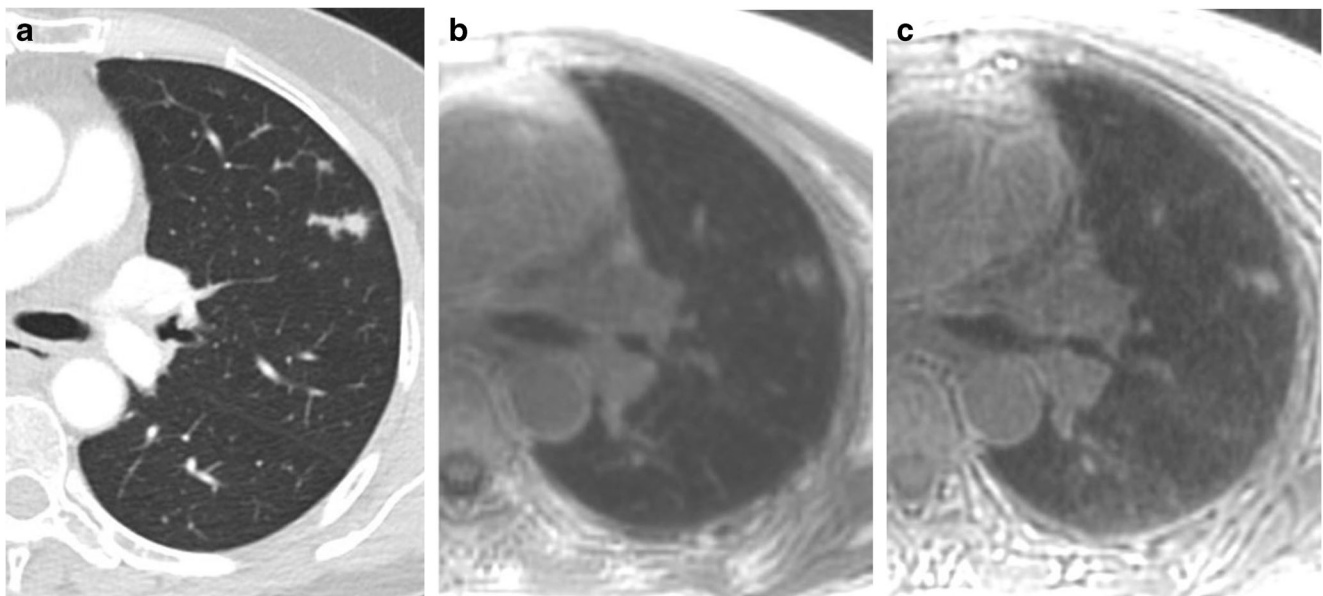


Fig. 5 Chest CT (a) and UTE (b) and ZTE (c) MR images at the level of the left upper-lobe bronchus in a 58-year-old female. There is a sub-centimeter nodule (6 mm) with irregular margin in the left upper lobe on CT. This nodule is more clearly delineated in ZTE sequence

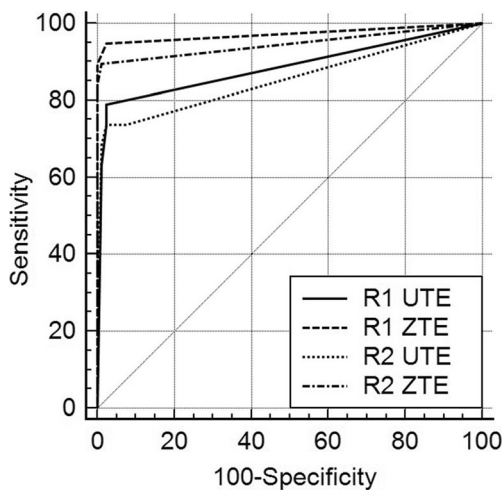


Fig. 6 Receiver operating characteristic curves for UTE and ZTE images in detecting sub-centimeter nodules on a lobe-by-lobe basis by two readers. AUCs were higher for ZTE (reader 1, 0.972; $p = 0.044$; reader 2, 0.946; $p = 0.045$) than those for UTE (reader 1, 0.885; reader 2, 0.855)

larger populations are required to confirm our preliminary results. Second, a comparison of lesion detection was performed in only a small number of solid nodules on a per-lobe base. According to the purpose of this study, we focused on the feasibility and image quality of ZTE compared with UTE. Lesion evaluation was performed quantitatively and qualitatively using a small number of sub-centimeter nodules being considered as the most important target of lung imaging. To validate the diagnostic performance and clinical relevance of ZTE in the evaluation of parenchymal lesions, further study is needed using a larger group with various lesions. Third, scan parameters of UTE and ZTE were not completely identical because of characters of each sequence and scanner system per se. Some parameters in ZTE such as the flip angle, receiver bandwidth, and segment TR were different from patient to patient. However, we tried to use the best optimized parameters for both sequences in each patient.

In conclusion, ZTE as a complementary sequence in routine clinical lung MR without contrast agent is feasible. It can be done in less than 3 min. This sequence can provide high-resolution structural information with better SNR for intrapulmonary structures and sub-centimeter nodules than UTE.

Funding The authors state that this work has not received any funding.

Compliance with ethical standards

Guarantor The scientific guarantor of this publication is Kyung Nyeo Jeon.

Conflict of interest The authors of this manuscript declare a relationship with GE Healthcare. GE Healthcare had provided them with 3D cones ultra-short TE research pulse. MJ Hwang and JS Lee are employees of

GE Healthcare (GE Healthcare Research, Korea). GE Healthcare had no role in the design and performance of the study, data analyses, or data interpretation.

Statistics and biometry No complex statistical methods were necessary for this paper.

Informed consent Written informed consent was obtained from all patients in this study.

Ethical approval Institutional Review Board approval was obtained.

Methodology

- Prospective
- Diagnostic or prognostic study
- Performed at one institution

References

1. Bergin CJ, Glover GM, Pauly J (1993) Magnetic resonance imaging of lung parenchyma. *J Thorac Imaging* 8:12–17
2. Gatehouse PD, Bydder GM (2003) Magnetic resonance imaging of short T2 components in tissue. *Clin Radiol* 58:1–19
3. Robson MD, Gatehouse PD, Bydder M, Bydder GM (2003) Magnetic resonance: an introduction to ultrashort TE (UTE) imaging. *J Comput Assist Tomogr* 27:825–846
4. Reichert IL, Benjamin M, Gatehouse PD et al (2004) Magnetic resonance imaging of periosteum with ultrashort TE pulse sequences. *J Magn Reson Imaging* 19:99–107
5. Robson MD, Benjamin M, Gishen P, Bydder GM (2004) Magnetic resonance imaging of the Achilles tendon using ultrashort TE (UTE) pulse sequences. *Clin Radiol* 59:727–735
6. Alsop DC, Hatabu H, Bonnet M, Listerud J, Gefter W (1995) Multi-slice, breathhold imaging of the lung with submillisecond echo times. *Magn Reson Med* 33:678–682
7. Takahashi M, Togao O, Obara M et al (2010) Ultra-short echo time (UTE) MR imaging of the lung: comparison between normal and emphysematous lungs in mutant mice. *J Magn Reson Imaging* 32:326–333
8. Ma W, Sheikh K, Svenningsen S et al (2015) Ultra-short echo-time pulmonary MRI: evaluation and reproducibility in COPD subjects with and without bronchiectasis. *J Magn Reson Imaging* 41:1465–1474
9. Ohno Y, Nishio M, Koyama H et al (2014) Pulmonary 3 T MRI with ultrashort TEs: influence of ultrashort echo time interval on pulmonary functional and clinical stage assessments of smokers. *J Magn Reson Imaging* 39:988–997
10. Johnson KM, Fain SB, Schiebler ML, Nagle S (2013) Optimized 3D ultrashort echo time pulmonary MRI. *Magn Reson Med* 70:1241–1250
11. Weiger M, Brunner DO, Dietrich BE, Müller CF, Pruessmann KP (2013) ZTE imaging in humans. *Magn Reson Med* 70:328–332
12. Alibek S, Vogel M, Sun W et al (2014) Acoustic noise reduction in MRI using Silent Scan: an initial experience. *Diagn Interv Radiol* 20:360–363
13. Weiger M, Wu M, Wurnig MC et al (2015) ZTE imaging with long-T2 suppression. *NMR Biomed* 28:247–254
14. Holdsworth SJ, Macpherson SJ, Yeom KW, Wintermark M, Zaharchuk G (2018) Clinical evaluation of silent T1-weighted MRI and silent MR angiography of the brain. *AJR Am J Roentgenol* 210:404–411
15. Gibiino F, Sacolick L, Menini A, Landini L, Wiesinger F (2015) Free-breathing, zero-TE MR lung imaging. *MAGMA* 28:207–221

16. Ko JP, Azour L (2018) Management of incidental lung nodules. *Semin Ultrasound CT MR* 39:249–259
17. MacMahon H, Naidich DP, Goo JM et al (2017) Guidelines for management of incidental pulmonary nodules detected on CT images: from the Fleischner Society 2017. *Radiology* 284:228–243
18. Weiger M, Wu M, Wurmig MC et al (2014) Rapid and robust pulmonary proton ZTE imaging in the mouse. *NMR Biomed* 27:1129–1134
19. Gurney PT, Hargreaves BA, Nishimura DG (2006) Design and analysis of a practical 3D cones trajectory. *Magn Reson Med* 55: 575–582
20. Bianchi A, Tibiletti M, Kjørstad Å et al (2015) Three-dimensional accurate detection of lung emphysema in rats using ultra-short and zero echo time MRI. *NMR Biomed* 28:1471–1479
21. Niwa T, Nozawa K, Aida N (2017) Visualization of the airway in infants with MRI using pointwise encoding time reduction with radial acquisition (PETRA). *J Magn Reson Imaging* 45:839–844
22. Yu J, Xue Y, Song HK (2011) Comparison of lung T2* during free-breathing at 1.5 T and 3.0 T with ultrashort echo time imaging. *Magn Reson Med* 66:248–254
23. Hatabu H, Alsop DC, Listerud J, Bonnet M, Gefter WB (1999) T2* and proton density measurement of normal human lung parenchyma using submillisecond echo time gradient echo magnetic resonance imaging. *Eur J Radiol* 29:245–252
24. Koyama H, Ohno Y, Kono A et al (2008) Quantitative and qualitative assessment of non-contrast-enhanced pulmonary MR imaging for management of pulmonary nodules in 161 subjects. *Eur Radiol* 18:2120–2131
25. Meier-Schroers M, Homs R, Skowasch D et al (2018) Lung cancer screening with MRI: results of the first screening round. *J Cancer Res Clin Oncol* 144:117–125
26. Ohno Y, Koyama H, Yoshikawa T et al (2016) Pulmonary high-resolution ultrashort TE MR imaging: comparison with thin-section standard- and low-dose computed tomography for the assessment of pulmonary parenchyma diseases. *J Magn Reson Imaging* 43: 512–532
27. Burris NS, Johnson KM, Larson PE et al (2016) Detection of small pulmonary nodules with ultrashort echo time sequences in oncology patients by using a PET/MR system. *Radiology* 278:239–246
28. Wiesinger F, Sacolick LI, Menini A et al (2016) Zero TE MR bone imaging in the head. *Magn Reson Med* 75:107–114
29. Price DL, De Wilde JP, Papadaki AM, Curran JS, Kitney RI (2001) Investigation of acoustic noise on 15 MRI scanners from 0.2 T to 3 T. *J Magn Reson Imaging* 13:288–293
30. Matsuo-Hagiyama C, Watanabe Y, Tanaka H et al (2017) Comparison of silent and conventional MR imaging for the evaluation of myelination in children. *Magn Reson Med Sci* 16:209–216